MONOSTATIC RADAR RESPONSE OF LUNAR PYROCLASTIC DEPOSITS. L. M. Jozwiak[1], A. M. Bramson[2, 3], G. A. Morgan[4], G. W. Patterson[1], S. S. Bhiravarasu[5], and L. M. Carter[2]. [1] Planetary Exploration Group, Johns Hopkins University Applied Physics Laboratory, Laurel, MD, USA. [2]University of Arizona, Lunar and Planetary Laboratory, [3]Purdue University, Department of Earth, Atmospheric, and Planetary Science, [4]Planetary Science Institute, Tucson, AZ, [4]Lunar and Planetary Science Institute, USRA, Houston, TX. (Corresponding author: lauren.jozwiak@jhuapl.edu)

Introduction: Pyroclastic deposits are the fine-grained, surface products of explosive volcanic eruptions. Consisting of glassy to crystalline blebs of magma (called pyroclasts); these deposits are important recorders of the volcanic and thermal evolution of a body, as well as the volatile state of the interior source region. On the Moon, returned samples of pyroclastic deposits [e.g. 1, 2] provided key evidence for the presence of water in the lunar interior [3], and remote sensing data suggest that these deposits might still serve as surface reservoirs of lunar water [4], making them possible targets for future lunar in-situ resource utilization (ISRU).

The identification of pyroclastic deposits on the Moon has traditionally required the presence of a low-reflectance deposit, frequently surrounding a central vent [after 5]. However, despite these common morphologic markers, there exist several locations where a pyroclastic deposit is known to exist without a low-reflectance deposit (e.g. Apollo 15), where vents exist without a low-reflectance deposit [6, 7], and where an explosive pyroclastic deposit cannot be compositionally distinguished from a small mare deposit (e.g. several entries in [5]). By emphasizing variations in particle size distribution and volume scattering properties, radar data have the potential to aide in both the characterization of existing pyroclastic deposits, and the possible identification of new pyroclastic deposits.

Using a global mosaic constructed from the Mini-RF monostatic dataset, we analyze the circular polarization ration (CPR) characteristics of both regional and localized pyroclastic deposits for a "radar pyroclastic signature". Our analysis will extend the analysis of [8] to additional regional pyroclastic deposits, and expand to localized pyroclastic deposits.

Lunar Pyroclastic Deposits: Lunar pyroclastic deposits are divided into two size-based categories: regional pyroclastic deposits which are greater than 1000 km^2 and typically lack identifiable source vents, and, localized pyroclastic deposits which are less than 1000 km^2 and typically surround identifiable source vents [5]. As observed using radar, pyroclastic deposits exhibit characteristically low backscatter returns, which is attributed to both the smooth surface of the deposits, and a lack of surface scatterers (such as rocks and boulders) within the deposit [e.g. 9, 10, 11].

Mini-RF Monostatic Analyses: The Mini-RF instrument onboard the Lunar Reconnaissance Orbiter, operated in a monostatic configuration from June of 2009 to December of 2010, both transmitting and receiving signal at the spacecraft. This provides a markedly different dataset from previous radar studies of pyroclastic deposits, which utilized terrestrially-based bistatic observations of the Moon [8-12]. During operation, Mini-RF acquired S-band (12.6 cm) observations of ~65% of the Moon, with near complete coverage at the lunar poles, and uniformly distributed, but sparser coverage at the equatorial and mid-latitudes. From these data, a global mosaic has been produced, with a resolution of 100 m/px, making this mosaic highly compatible with the LROC WAC 100 m/px global mosaic [13].

The standard list of lunar pyroclastic deposits is found in Table 1 of [5]. Of the 75 deposits in this database, 46 deposits have some amount of Mini-RF monostatic coverage (50% of regional deposits and 66% of localized deposits). We have used a combination of the LROC WAC 100 m/px global mosaic and the Clementine UVVIS global 200 m/px color ratio mosaic to generate shapefile outlines of deposit extent. The ArcGIS program then allows us to extract and analyze the Mini-RF monostatic data that fall within each mapped deposit shapefile.

The Aristarchus pyroclastic deposit (26.7° N, 52.3° W) (Fig. 1) is the largest pyroclastic deposit on the Moon [5], and spans over 20 individual radar collects (Fig. 1). We extracted CPR values from the entire deposit, a smaller subsection of the deposit, and a nearby non-pyroclastic mare region. Because of known issues with data processing and power fall-off at the edges of data collects [14], we also sampled a subsection of the deposit contained in a single observation. The results for each shapefile are show in Table 1, along with the standard deviation of pixel values for each shapefile. Overall, they indicate that while the entire pyroclastic deposit has nominally lower CPR, this is not significantly lower than nearby mare regions. This observation is similar to [15], where a bistatic data showed nominally lower backscatter for the Aristarchus pyroclastic deposit, but no significant changes in CPR. Comparing data from a single radar strip to the averaged data, we observe significantly lower backscatter return, and smaller standard deviations in the single observation. This suggests that qualitative observations of power roll-off at the edges of data collects, combined with higher backscatter contributions from small craters might be

combining to decrease the measured distinction between pyroclastic deposit and non-pyroclastic deposit CPR. We also observe this pattern at the Sinus Aestuum pyroclastic deposit, where the average CPR of the full deposit is 0.44, while a single observation subsection has a CPR of 0.31.

We also applied this analysis to two localized pyroclastic deposits within Alphonsus crater (Fig. 2), the Alphonsus East (14.3° S, 2° W) and Alphonsus West (13.6° S, 4° W) deposits. These small deposits are near the resolution of the Mini-RF monostatic data (which varies from 30m–100m), and qualitative observations do not suggest the presence of a low backscatter deposit, despite the clearly observable low-reflectance deposit observable in LROC WAC data. Analyses of the Mini-RF CPR data support this qualitative observation (Table 1), showing no distinction between the backscatter of the pyroclastic deposits and the floor of the crater.

Conclusions and Ongoing Work: Our preliminary results indicate that while lunar pyroclastic deposits may qualitatively display low CPR, the statistical significance and uniqueness of this signature is more difficult to characterize. Additionally, preliminary analysis suggests that measurements are very sensitive to data location, and that significant care should be taken to ensure that the edges of data strips and other geologic features should be avoided when characterizing the overall CPR of a deposit.

With the results from our preliminary analysis in mind, we are continuing to analyze the CPR of all 46 deposits with Mini-RF data coverage in a variety of ways. Our analyses will continue to include fully averaged values, subsection values (for regional deposits), and new shapefiles consisting of the interior high-power returns for each data collect containing pyroclastic material. By analyzing all of these data, we hope to establish more firmly whether there exists a characteristic lunar pyroclastic CPR value. Furthermore, we are targeting additional pyroclastic deposits for bistatic radar acquisition. These new bistatic data will be used for further comparison with the monostatic results, and to explore the phase angle dependence of any observed "pyroclastic signal".

References: [1] Ridley, W. I., et al. (1973) *Phys. Earth Planet Int., 7*, 133-136. [2] Heiken, G. and McKay D. S. (1974) *Proc. Lunar Planet. Sci. Conf., 5*, 843-860. [3] Saal, A. E., et al. (2008) *Nature, 454*, 192-195. [4] Milliken, R. E. and Li, S. (2017) *Nature Geosci., 10*, 561-565. [5] Gaddis, L. R., et al. (2003) *Icarus, 161*, 262-280. [6] Gustafson, J. O., et al. (2012) *JGR Planets, 117*, E00H25. [7] Jozwiak, L. M., et al. (2016) *LPSC XLVII, Abstract #1169*. [8] Carter, L. M., et al. (2009) *JGR Planets, 114*, E11004. [9] Pieters, C., et al. (1973) *JGR, 78*, 5867-5875. [10] Zisk, S. H., et al. (1977) *The Moon, 17*, 59-99. [11] Gaddis, L. R., et al. (1985) *Icarus, 61*, 461-489. [12] Campbell, B. A., et al. (2008) *Geology, 36*, 135-138. [13] Speyerer, E. J., et al. (2011) *LPSC XLII, Abstract #2387*. [14] Carter, L. M., et al. (2017) *IEEE Trans. On Geosci. and Remote Sens., 55*, 1915-1927. [15] Patterson, G. W., et al. (2017) *Icarus, 283*, 2-19.

Tables:

Table 1: Mini-RF Monostatic CPR values

Deposit Name	Avg. CPR	Std. Dev
Aristarchus Single Observation Subset	**0.34**	**0.08**
Aristarchus Subset	**0.43**	**0.12**
Aristarchus Full	**0.41**	**0.11**
Aristarchus Regional Mare	**0.43**	**0.06**
Alphonsus W Vent	**0.46**	**0.09**
Alphonsus E Vent	**0.4**	**0.06**
Alphonsus Crater floor	**0.41**	**0.08**

Figures:

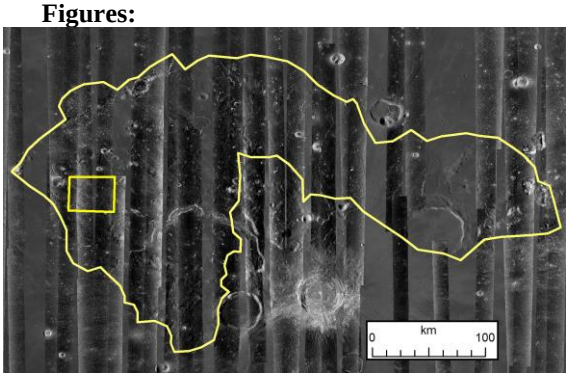

Figure 1: Mini-RF monostatic coverage (strips) of the Aristarchus pyroclastic deposit (large outline), analysis subsection (rectangle), over LROC WAC 100m/px mosaic.

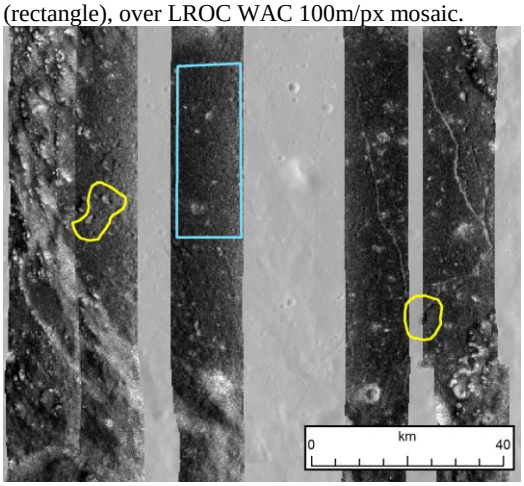

Figure 2: Analysis regions in Alphonsus crater, including the west (left) and east (right) localized pyroclastic deposits, and non-pyroclastic deposit crater floor (center rectangle).